Modeling and Parameter Estimation of the Human Index Finger

Robert N. Rohling and John M. Hollerbach

Biorobotics Laboratory, McGill University
3775 University St., Montreal, Quebec H3A 2B4

Abstract

Precise teleoperation of dextrous robotic hands by hand masters requires an accurate human hand model. A kinematic model of a human index finger is developed as an example for human hand modeling. The parameters of the model are determined by open-loop kinematic calibration. Singular value decomposition is used as a tool for analyzing the kinematic model and the identification process. Accurate and reliable results are obtained only when the numerical condition is minimized through parameter scaling, model reduction and pose set selection. The identified kinematic parameters show the kinematic model and calibration procedure have an accuracy on the order of a few millimeters.

1 Introduction

Advances in the field of telemanipulation using dextrous slave robotic hands and sophisticated hand masters have made it necessary [9, 12] to develop a kinematic model of each operator's hand. As telemanipulation tasks become more delicate and difficult, accuracy of the human hand model is required to achieve accurate control of the slave robotic hand.

The main difficulty of devising a hand model arises from model parameter identification. Because of the very complex structure of the human hand, a tractable hand model must incorporate a number of simplifications. Yet studies of the hand are limited by the fact that some of the structures such as the joint articular surfaces are not easily accessible and vary for each individual.

No other kinematic parameter identification method other than external caliper measurement of the finger lengths has yet been used in the dextrous hand teleoperation field. The parameters are poorly identified by the caliper measurement method because of a lack of accurate distinguishable bony landmarks. The biomechanics field [2, 3, 11, 16] often makes use of roentenograms, MRI and CT scans for model parameter determination. Single scans also don't achieve accurate estimates because the bone link lengths are not equal to the effective link lengths and the center of rotation and the direction of its axis are difficult to determine. Multiple three dimensional scans require extensive computations to identify the kinematic parameters. Multiple source roentenogram machines, MRI and CT scanners are also typically unavailable to users in the field of teleoperation. A method for easily and accurately identifying the kinematic parameters is required.

Figure 1: Utah Dextrous Hand Master

The Utah Dextrous Hand Master (UDHM, Figure 1) and the OPTOTRAK^{TM} (Northern Digital Inc, Waterloo, ON, Canada) position tracker are the measurement tools used to perform open-loop kinematic calibration - a well-known calibration technique - to identify the kinematic parameters of the author's (RNR) index finger. After a brief review of the anatomy of the human hand, this paper describes the derivation of a kinematic model of the human index finger. Other fingers of the hand may be similarly modeled to obtain a complete model of the human hand. In addition to the teleoperation field an accurate hand model may benefit the fields of biomechanics, virtual reality and haptic interfaces.

2 Human Hand Kinematics

2.1 Overview of Human Hand Anatomy

The skeleton of the wrist consists of eight carpal bones arranged in approximately two rows (Figure 2). The thumb extends from the trapezium of the carpus and consists of a metacarpal bone and two phalanges. The index, middle, ring and pinkie fingers each consist

1050-4729/94 $03.00

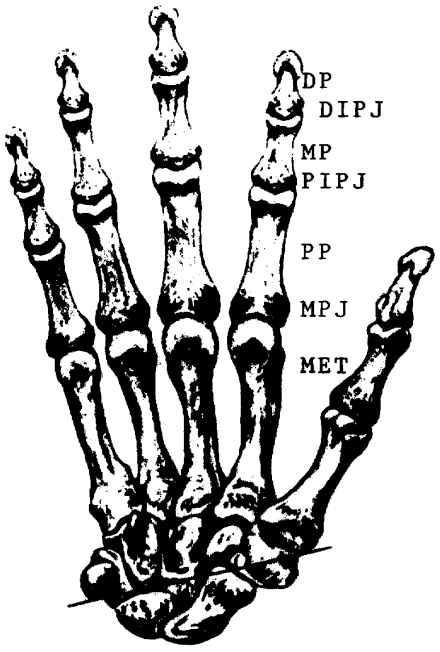

Figure 2: Volar aspect of the human hand skeleton. The index finger links are comprised of a metacarpal (MET), proximal phalanx (PP), middle phalanx (MP), and distal phalanx (DP). The finger joints are labeled as the metacarpophalangeal joint (MPJ), proximal interphalangeal joint (PIPJ) and distal interphalangeal joint (DIPJ). (*Kaplan's Functional and Surgical Anatomy of the Human Hand*[13]).

of a metacarpal bone and three phalanges: proximal, medial and distal.

A study of hand anatomy from a kinematics viewpoint requires analysis of both the skeletal and the capsuloligamentous structure. The hand may be considered [2] as a linkage system of intercalated bony segments. These segments define the fingers and palm and allow motion through movement between bone segments. Joint movement is described by the bone segments moving along articulated surfaces. The joints are spanned by soft tissue: ligaments, tendons and muscles. Joint motion is produced by muscle force and constrained by both soft tissue (including muscle) and bony articulation. These constraints allow simplifications to be made about gross finger motion.

2.2 Kinematic Model

The bulk of research concerning hand modeling comes from the field of biomechanics. Without the muscles and capsuloligamentous structure - defined by the synovial joint capsule and finger ligaments - each joint would contain 6 degrees of freedom (DOF). The soft tissue and bony articulation constraints allow the joints to be modeled as Hookean hinge joints [2, 3, 14].

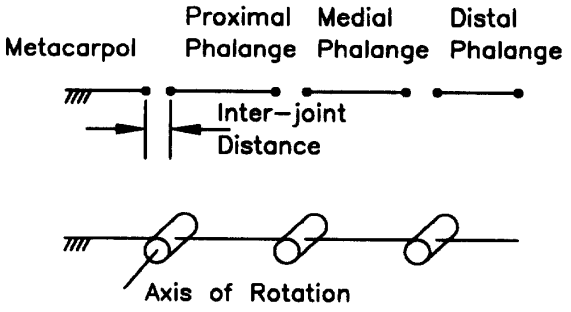

Figure 3: Real finger links and the mechanical hinge model

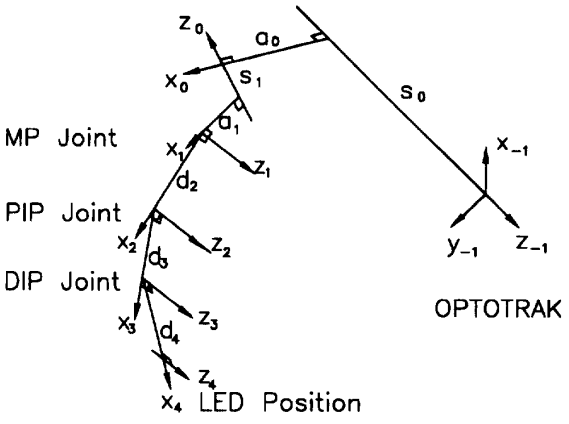

Figure 4: Denavit-Hartenberg and Hayati Coordinate Systems of the Index Finger. Parameters α_i , θ_i, and β_i are omitted for clarity.

The PIPJ and DIPJ are modeled as having 1 DOF and the MPJ as 2 DOF. A hinge joint model is commonly used in hand modeling because it has been shown [2] that the inter-joint distances remain fairly constant during flexion/extension. The real finger and the mechanical hinge model are depicted in Figure 3. This paper describes a model of the index finger; the other fingers may be similarly modeled.

Following traditional practice of modeling robot kinematics, a series of reference frames are selected for each of the index finger joints. The Denavit-Hartenberg (DH) [4] convention is used for the first two frames and a modified convention [5] (referred to hereafter as the Hayati convention) for the next three frames (Figure 4). The Hayati convention is chosen because the three distal joints have nearly parallel axes and a DH convention results in poorly identifiable parameters.

The transforms between each of the coordinate frames are described as:

$^{-1}\mathbf{T}_0 = \mathbf{Rot}_z(\theta_0)\mathbf{Trans}_z(s_0)\mathbf{Trans}_x(a_0)\mathbf{Rot}_x(\alpha_0)$
$^{0}\mathbf{T}_1 = \mathbf{Rot}_z(\theta_1)\mathbf{Trans}_z(s_1)\mathbf{Trans}_x(a_1)\mathbf{Rot}_x(\alpha_1)$
$^{1}\mathbf{T}_2 = \mathbf{Rot}_z(\theta_2)\mathbf{Trans}_x(d_2)\mathbf{Rot}_x(\alpha_2)\mathbf{Rot}_y(\beta_2)$
$^{2}\mathbf{T}_3 = \mathbf{Rot}_z(\theta_3)\mathbf{Trans}_x(d_3)\mathbf{Rot}_x(\alpha_3)\mathbf{Rot}_y(\beta_3)$
$^{3}\mathbf{T}_4 = \mathbf{Rot}_z(\theta_4)\mathbf{Trans}_x(d_4)\mathbf{Rot}_x(\alpha_4)\mathbf{Rot}_y(\beta_4)$
where

$^{i-1}\mathbf{T}_i$ = homogeneous transform matrix between reference frame i-1 and i

$\mathbf{Rot}_k(angle_i)$ = rotation of $angle_i$ about the k axis

$\mathbf{Trans}_k(distance_i)$ = translation of $distance_i$ along the k axis

3 Open-Loop Kinematic Calibration

3.1 Method

To accurately determine the finger kinematic parameters, open loop kinematic calibration [1] is used. An external measurement system is used to measure the endpoint of the index finger and the measuring instrument's coordinate system (labeled -1 for convenience) is added to the chain of systems used for the finger joints. The endpoint may be calculated if the fixed kinematic parameters are known and the variable ones are measured. This calculation is done through homogeneous transforms:

$$^{-1}\mathbf{d}_{endpoint} = {}^{-1}\mathbf{T}_0\,{}^{0}\mathbf{T}_1\,{}^{1}\mathbf{T}_2\,{}^{2}\mathbf{T}_3\,{}^{3}\mathbf{T}_4\,{}^{4}\mathbf{d}_{endpoint}$$

where

$^{4}\mathbf{d}_{endpoint} = [0\ 0\ 0\ 1]^T$

$^{-1}\mathbf{d}_{endpoint}$ = position of the fingertip endpoint calculated from link parameters with respect to the -1 reference frame

This endpoint position vector is subtracted from the directly measured endpoint position (measured by the OPTOTRAK^{TM} position tracker) for m poses to yield an error vector of stacked endpoint position errors:

$$\begin{bmatrix} {}^{-1}\Delta\mathbf{d}_1 \\ \vdots \\ {}^{-1}\Delta\mathbf{d}_m \end{bmatrix} = \begin{bmatrix} \mathbf{C}_1 \\ \vdots \\ \mathbf{C}_m \end{bmatrix} \Delta\phi$$

or more compactly

$$\mathbf{e} = \mathbf{D}\Delta\phi$$

where

$^{-1}\Delta\mathbf{d}_p$ = the pose p error vector between measured endpoint position and endpoint position calculated from link parameters

$\mathbf{C}_p$ = Jacobian matrix for pose p with respect to the kinematic parameters written with respect to the -1 reference frame (axes labeled -1)

$\Delta\phi$ = vector of variations in kinematic parameters

$\mathbf{C}$ is prohibitively difficult to determine by direct differentiation but is easily evaluated by screw vector analysis [15]:
for i = 0,1 (DH parameters)

$$^{-1}\Delta\mathbf{d} = \Delta\Theta_i(\mathbf{z}_{i-1} \times \mathbf{b}_i) + \Delta\alpha_i(\mathbf{x}_i \times \mathbf{b}_{i+1}) + \Delta a_i(\mathbf{x}_i) + \Delta s_i(\mathbf{z}_{i-1})$$

and for i = 2,3 and 4 (Hayati parameters)

$$^{-1}\Delta\mathbf{d} = \Delta\Theta_i(\mathbf{z}_{i-1} \times \mathbf{b}_i) + \Delta d_i(\mathbf{Rot}_z(\Theta_i)\mathbf{x}_{i-1}) + \Delta\alpha_i((\mathbf{Rot}_z(\Theta_i)\mathbf{x}_{i-1}) \times \mathbf{b}_{i+1}) + \Delta\beta_i(\mathbf{y}_i \times \mathbf{b}_{i+1})$$

where $\mathbf{b}_i$ is the vector from the i-1 coordinate frame to the endpoint.

The parameters ϕ are determined by an iterative process to minimize $\mathbf{e}$ whereby $\Delta\phi \rightarrow 0$ and the parameters converge to stable values. At each stage the Jacobian is evaluated with the current parameters.

3.2 Calibration Equipment

A light emitting diode (LED) was attached to a cast affixed to the fingernail of the index fingertip. The cast was prepared by closely wrapping the tip of the index finger with orthopaedic casting tape into the shape of a thimble and hydrating to set the cast. An aluminum and epoxy plug was made to hold the cast during subsequent machining. The cast was machined on a CNC mill to cut a circular recess into the side of the cast at the location of the end of the distal phalanx. Also excess cast material was removed to minimize bulk and mass. The cast was then coated in epoxy for greater strength and the LED was placed in the recess (Figure 5). The result is a low profile cast weighing only 2.6 grams.

The OPTOTRAK^{TM} is a position tracking device which tracks infrared LED emitters by three fixed CCD cameras. The OPTOTRAK^{TM} has a stated accuracy of 0.15 mm and a resolution of 0.01 mm at a distance of 2.5 m between the thimble LED and the cameras. Low noise levels during tests yield a resolution of slightly greater than 0.01 mm.

To measure the DH variables θ_1, θ_2, θ_3, and θ_4 the instrumented UDHM glove is worn by the subject during calibration. The UDHM measures motion of the thumb, index, middle and ring fingers via a carbon-fibre exoskeleton attached to an elasticized glove (Figure 1) The exoskeleton is comprised of 3 pairs of parallel-link mechanisms spanning the length of each finger and attached to an immobile base on the back of the hand. Pads are adhered to the glove surface above the three finger links of each finger and connected to the parallel linkages. Rotation of adjacent pads or rotation of the proximal pad with respect to the immobile base yields an angular motion between pairs of parallel linkages (Figure 6) and is measured

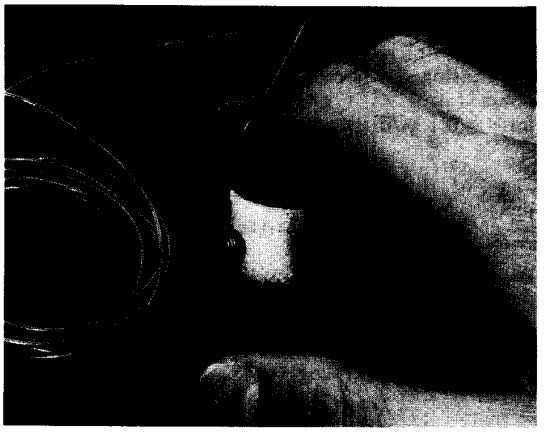

Figure 5: Index finger cast and LED

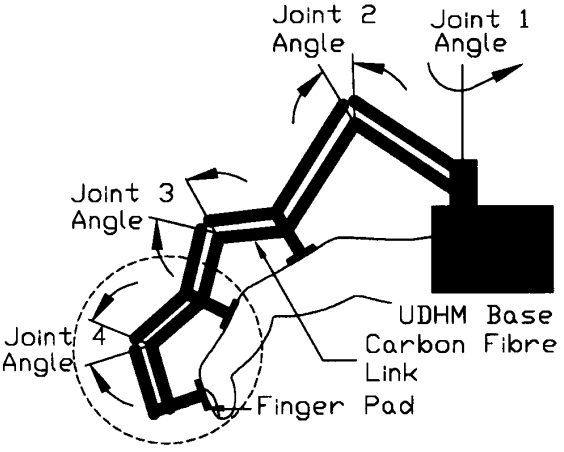

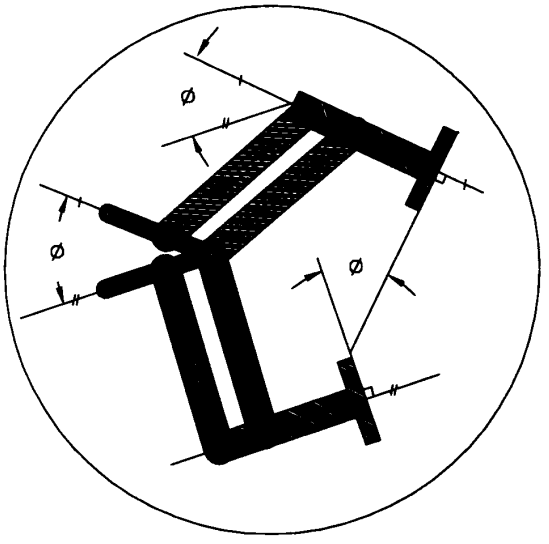

Figure 6: Utah Dextrous Hand Master

by Hall-effect sensors. Abduction/adduction of each finger rotates the series of parallel linkages about a perpendicular axis and is measured by Hall-effect sensors located in the base.

The nature of the parallel link mechanism means θ_2, θ_3, and θ_4 are directly measured, but θ_1 is measured by a linear fit of the base joint sensor readings. The slope and offset of the base joint readings are required because the base joint sensor rotates about an axis which is not perfectly coincident with the human MP joint. The slope and offset are added to the list of parameters to be identified (Table 1). The other joint sensors are calibrated before each test by mounting on a calibrated aluminum artificial finger joint.

The UDHM base is placed at a fixed position and orientation in front of the OPTOTRAK^{TM} cameras to record the LED position with respect to an immobile palm. The subject attaches the cast to the index finger and inserts the hand into the glove. The LED is clearly visible through the mesh-like material of the glove.

The UDHM angles are read at 25 Hz by a 12 bit A/D converter connected to the CONDOR [8] real time computer system. Linked to CONDOR is the OPTOTRAK^{TM} computer which records the LED position at 25 Hz in sync with CONDOR. The UDHM angles and LED position are converted into MATLAB^{TM} (The MathWorks Inc, Natick, MA) format to perform the calibration analysis.

3.3 Parameter Scaling

The large differences in the magnitudes of the identifiable kinematic parameters and their effect upon endpoint position produce an ill-conditioned identification problem. Parameter scaling is implemented to improve the conditioning by introducing a scaling matrix:

$$\mathbf{e} = \mathbf{D}\Delta\phi \quad \rightarrow \quad \mathbf{e} = (\mathbf{DH})(\mathbf{H}^{-1}\Delta\phi)$$

where

$\mathbf{H}$ = diagonal matrix of scaling factors t_j

The t_j scaling values are traditionally chosen by Euclidean norms of the columns of $\mathbf{D}$ [6]. This method is simple to implement because it requires no a priori statistical information. One drawback to Euclidean norm column scaling is that very large scale factors can arise from small Euclidean norms of poorly identified parameters, resulting in strong amplification of the uncertainties of $\mathbf{C}$ [10].

Model based scaling is preferred because it results in better numerical conditioning, does not depend upon the calibration pose sets and can be calculated prior to calibration. The scale factors are calculated as follows:

For a large pose set $p \in \{1, \ldots, 500\}$ created without positional or orientational constraints, define:

$$^{-1}\Delta \mathbf{d}_p = \mathbf{C}_p \Delta\phi$$

$$t_j(p) = \frac{1\,mm}{||column_j(\mathbf{C}_p)||}$$

where

$1mm$ is the expected endpoint positional error.

t_j represents the parameter deviation that causes a 1 millimeter endpoint displacement when using a first order approximation.

If the pose set p is sufficiently large and descriptive of all possible poses then select t_j as follows:

$$t_j = \min_p t_j(p)$$

The value t_j is called the extremal scaling value and yields good numerical conditioning.

3.4 Model Optimization

There is a trade-off between model reduction to increase numerical condition and the decrease in pose accuracy by model simplification. The model optimization proceeds until an acceptable numerical condition is achieved through a minimal deletion of model parameters.

There are 18 fixed kinematic parameters (Table 1) used to determine the endpoint frame on the index finger - 16 DH and Hayati parameters and the scale and offset for the base joint. Parameters α_4 and β_4 are unidentifiable because they have no effect on endpoint position, only orientation. They may be set to zero and removed from list of identifiable parameters. Parameters α_2, α_3, β_2 and β_3 simply are not identifiable due to the nature of the rigid UDHM exoskeleton so they are also set to zero and removed from the list of identifiable parameters.

The base joint sensor contains a significant level of hysteresis so calibration of the index finger without abduction/adduction (planar) movement is performed to eliminate the contribution from this sensor. Singular value decomposition (SVD) of the Jacobian of the remaining 12 identifiable parameters for planar finger motion reveal a rank of 9.

$$\mathbf{D} = \mathbf{USV}^T$$

where

$\mathbf{U}$ = matrix of the left singular vectors of $\mathbf{D}$

$\mathbf{S}$ = diagonal matrix of ordered singular values σ_k

$\mathbf{V}$ = matrix of the right singular vectors of $\mathbf{D}$

j	Complete Model	Optimized Model
1	Θ_0	Θ_0
2	α_0	α_1
3	α_1	s_0
4	s_0	s_1
5	s_1	a_1
6	a_0	d_2
7	a_1	d_3
8	d_2	d_4
9	d_3	b
10	d_4	
11	α_2	
12	α_3	
13	α_4	
14	β_2	
15	β_3	
16	β_4	
17	m	
18	b	

Table 1: Complete list of the fixed DH and Hayati parameters and a list of the optimized model parameters.

diagonal element	singular values of unscaled D	singular values of scaled, optimized D
1	8.670×10^3	4.780
2	4.170×10^3	2.494
3	1.136×10^3	2.308
4	7.645×10^2	2.109
5	3.250×10^1	1.828
6	2.584×10^1	1.754
7	2.090×10^1	1.292
8	1.284×10^1	1.065
9	3.373×10^0	0.247
10	4.929×10^{-13}	
11	1.732×10^{-14}	
12	0	

Table 2: Singular values of the unscaled 12 parameter D matrix and for the scaled matrix D of the optimized model.

Rank deficiencies will not produce a unique solution for the identified parameters. Table 2 contains the list of singular values of the unscaled D matrix for the remaining 12 parameters. Three parameters must be removed from the list of identifiable parameters. A low condition number κ is required for good identifiability because it is an indication of how errors are amplified during identification.

$$\kappa = ||\mathbf{D}||||\mathbf{D}^{-1}|| = \sigma_1/\sigma_r$$

where

$\mathbf{D}^{-1}$ = pseudo-inverse of D

σ_1 = largest singular value

σ_r = smallest singular value

Number of Parameters	Reduction Method	Condition Number
12		∞
11	eliminate m (j=17)	5.00×10^{17}
10	eliminate α_0 (j=6)	2.20×10^{16}
9	eliminate α_0 (j=2)	2.86×10^{3}
9	parameter scaling	19.3
9	Calibration Trial	61.9

Table 3: Reduction of condition number of simulations through model optimization and scaling. Condition number of actual calibration data using a scaled optimum model is listed at bottom.

Inspection of the last column of V shows that the parameter m must be removed. The SVD is recalculated after the removal of m. Parameters α_0 and a_0 are also removed because their removal results in the lowest condition number. The singular values of the scaled, optimized model D are listed in Table 2. After scaling and model reduction, the condition number of simulated data is 19.3. A condition number lower than 100 has been suggested [10] as the largest acceptable condition number for reliable results. As Table 3 shows, the scaled D matrix for real calibration data results in a condition of 61.9, higher than the simulated data because of the use of slightly less than full joint ranges.

3.5 Pose Set Optimization

Unlike most robots, the human finger is not capable of attaining arbitrary poses. Each joint is limited to approximately 90^o of flexion/extension movement. Furthermore, each joint cannot be flexed through its range independent of other joint movements. For this reason, a pose set was chosen that is simply a typical finger curling/uncurling motion (Figure 8).

Simulations of this movement are performed to observe how the condition number depends upon the number of poses. Another good measure of identifiability is the observability index **O** [7]:

$$\mathbf{O} = \frac{\sqrt[L]{\sigma_1 \cdot \sigma_2 \cdots \sigma_L}}{\sqrt{m}}$$

where L is the number of identifiable parameters, and m is the number of poses.

A low condition number and a high observability index are required, so by inspection of Figure 7, 500 poses is chosen as a sufficient number to guarantee reliable results.

3.6 Simulations

Simulations of 500 poses are performed to ensure error-free computer code, to determine the robustness of the identification procedure to poor initial estimates of the parameters and noise on the UDHM and OPTOTRAK readings. Using initial parameter estimates in error of up to 80% still results in convergence of the iterative non-linear least squares procedure to repeatable and accurate results. UDHM and OPTOTRAK noise at expected levels (standard deviations of 0.035 radians and 0.5mm respectively) result in errors of parameter identification of less than 0.036 radians for the angle parameters and 0.5 mm for the length parameters.

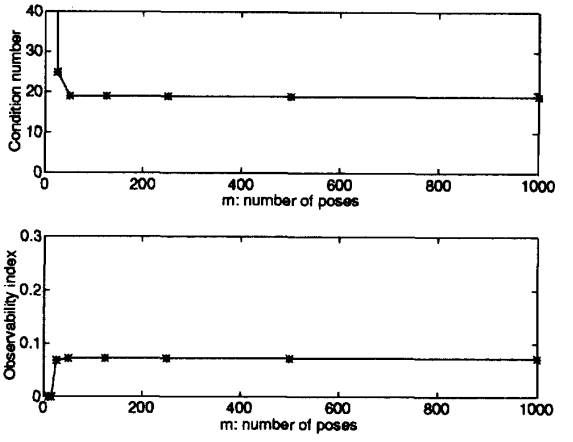

Figure 7: Condition number and observability index as a function of number of poses.

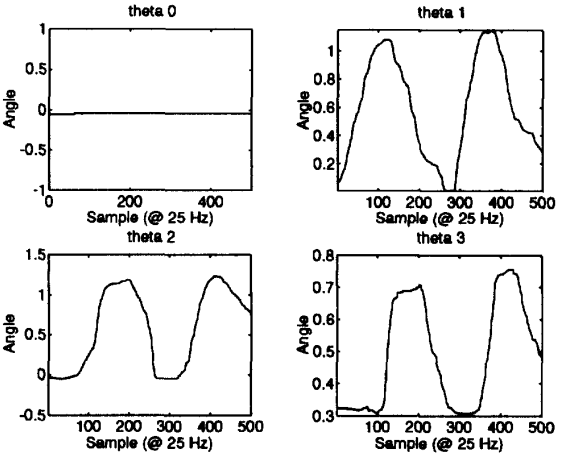

Figure 8: Joint angle data for calibration trial #1

4 Results

4.1 Test Data

The author's (RNR) index calibration data are shown in Figures 8 and 9.

A number of additional LEDs are placed on the exoskeleton to ensure that the finger is undergoing planar motion during calibration. LEDs are also placed on the UDHM base to detect base movement. The

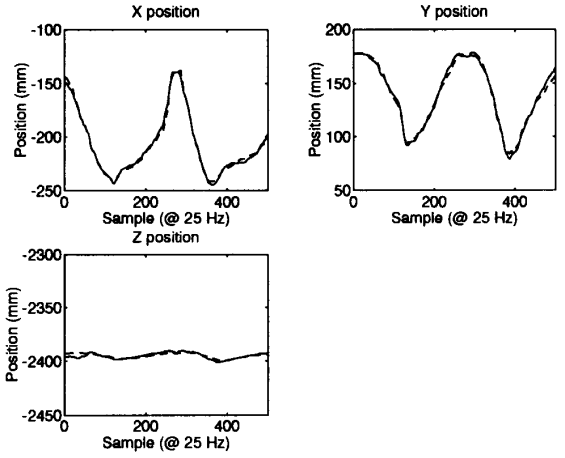

Figure 9: Measured OPTOTRAK endpoint position data (solid line) and endpoint position calculated from UDHM measurements and the identified parameters from the least squares fit (dashed line).

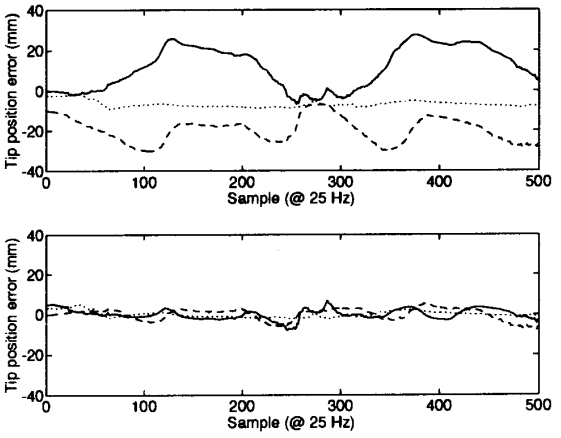

Figure 10: Endpoint errors calculated using initial parameter estimates (top) and the identified parameters. Solid line is the ${}^{-1}\mathbf{x}_{error}$, dashed line is ${}^{-1}\mathbf{y}_{error}$ and dotted line is ${}^{-1}\mathbf{z}_{error}$.

Parameter	Initial Estimate	Calibrated Value
Θ_0	1.57	1.3458
α_1	-1.57	-1.5418
s_0	-2405	-2397.4
s_1	-139	-171.94
a_1	0	-30.584
d_2	40	39.079
d_3	30	43.534
d_4	20	11.179
b	8×10^{-2}	7.7685×10^{-2}
$d_2 + d_3 + d_4$	90.0	93.8
VAF (%)	52.9	99.0
RMS error (mm)	9.70	1.42

Table 4: Initial parameter estimates, identified parameter values and measures of model fit.

base movement is measured to have a standard deviation of 0.03 mm.

4.2 Parameter Identification

The iterative identification procedure converged within 20 iterations from a number of different initial parameter estimates, indicating a global minimum. The resulting endpoint errors are shown in Figure 10. Common measures [1] of the model fit are the Variance Accounted For (VAF) and the Root Mean Squared (RMS) error of the endpoint position. The identified parameter values and the measures of model fit are listed in Table 4.

A second calibration test is done to demonstrate repeatability. The first five parameters listed in Table 4 describe the location and orientation of the base knuckle joint which vary slightly between tests. The d_2, d_3 and d_4 parameters describe the human finger link lengths and should not vary. The d_2, d_3 and d_4 are found to be repeatable between the first and second test by 5.7mm, 0.7mm and 2.1mm respectively. The sum $(d_2 + d_3 + d_4)$ describe the total finger length and is found to be 93.8 and 90.8 for the first and second tests - a difference of 3.0mm.

4.3 Sources of Error

The level of repeatability in parameter identification is shown to be on the order of a few millimeters. The parameter identification problem is limited by a number of error sources:

- the Hall-effect sensors are calibrated using an aluminum artificial Hookean finger joint and have a typical non-linearity error of $\pm 2^o$.
- the UDHM exoskeleton undergoes slight movement with respect to the human skeleton because of the soft nature of the fleshy attachment locations.
- the base joint of the exoskeleton - used to measure abduction/adduction - has a level of hysteresis of 10^o. When no detectable change is recorded in the base joint sensor signal, the finger may still not be undergoing planar motion by an error of up to $\pm 5^o$.
- the level of noise and drift from OPTOTRAK sensor is measured to have a maximum of 0.15mm.
- the location of the base knuckle joint is not perfectly fixed during the calibration test.
- the thimble experiences movement with respect to the human skeleton by up to $\pm$ 0.5mm.

- the human finger is not perfectly modeled by the DH and Hayati coordinate systems.

The last listed error source is the most important but most difficult to quantitatively measure. Implicit in the entire calibration procedure is that the index finger does closely approximate the proposed finger model. Yet the DH and Hayati parameters do not remain perfectly constant during flexion/extension because the center of rotation of the joints does not remain perfectly constant during motion. These unmodeled parameter changes contribute to the identification error.

5 Conclusions

The main success of these experiments is the ability to perform a common robot calibration technique - open loop calibration - to the human finger. It is shown that if the procedure includes steps to minimize measurement error, maximize problem conditioning, and perform model and pose set optimization then identifiability and reliability are obtained. The accuracy of determination of parameters to within a few millimeters shows the limitations of the finger model as well as the difficulty in obtaining accurate external measurements of finger movement. This level of accuracy still surpasses the traditional parameter determination techniques and can improve the accuracy of teleoperation tasks. This method of modeling should also increase the accuracy of solutions to problems in biomechanics, virtual reality and haptic interfaces.

6 Acknowledgements

Support for this research was provided by Office of Naval Research Grant N00014-90-J-1849, and by the Natural Sciences and Engineering Research Council (NSERC) Network Centers of Excellence Institute for Robotics and Intelligent Systems (IRIS). Personal support for JMH was provided by the NSERC/Canadian Institute for Advanced Research (CIAR) Industrial Chair in Robotics and for RNR by an NSERC Postgraduate Scholarship.

References

[1] C. H. An, C. G. Atkeson and J. M. Hollerbach, *Model Based Control of a Robot Manipulator.* Cambridge, MA: MIT Press, 1988.

[2] E.Y.S. Chao, K. An, W.P. Cooney III, R.L. Linschied, *Biomechanics of the Hand.* World Scientific, 1989.

[3] W.P. Cooney III, M.J. Lucca, E.V.S. Chao, and R.L. Linscheid, "The kinesiology of the thumb trapeziometacarpol joint," *J. Bone and Joint Surgery*, vol. 63-A, pp. 1371-1381, 1981.

[4] J. Denavit and R.S. Hartenberg, "A kinematic notation for lower pair mechanisms based on matrices," *J. Applied Mechanics*, vol. 22, pp. 215-221, 1955.

[5] S. Hayati and M. Mirmirani, "Improving the absolute positioning accuracy of robot manipulators," *Journal of Robotic Systems*, vol. 2(5), pp. 397-413, 1985.

[6] C.L. Lawson and R.J. Hanson, *Solving Least Squares Problems.* Englewood Cliffs, N.J.: Prentice - Hall, pp. 180-198, 1974.

[7] C.H. Menq, J.H.Borm and J.Z. Lai, "Identification and observability measure of a basis set of error parameters in robot calibration," *J. Mechanisms, Transmissions, and Automation in Design*, vol. 111, pp. 513-518, 1989.

[8] S. Narasimhan, D.M. Siegel, and J.M. Hollerbach, "Condor: an architecture for controlling the Utah - MIT Dextrous Hand," *IEEE Trans. Robotics and Automation*, vol. 5, pp. 616-627, 1989.

[9] R.N. Rohling and J.M. Hollerbach, "Optimized Fingertip Mapping for Teleoperation of Dextrous Robot Hands," in *IEEE Int'l Conf. of Robotics and Automation*, pp. 769-775, 1993.

[10] K. Schroer, L. Uhl, S. Albright, and M Huttenhofer, "Ensuring solvability and analyzing results of the nonlinear robot calibration problem," in *Second International Symposium on Measurement and Control in Robotics*, Tsukuba Science City, Japan, pp. 851-858, 1992.

[11] C.F. Small, J.T. Bryan, D.R. Pichora, I.L. Dwosh and P.M. Griffiths, "Precision of bone landmarks in characterizing hand and wrist position," in *Canadian Medical and Biomedical Engineering Conference*, Toronto, pp. 24-25, 1992.

[12] T.H. Speeter, "Transforming human hand motion for telemanipulation," *Presence: Teleoperators and Virtual Environments*, vol. 1, pp. 63-79, 1992.

[13] M. Spinner, M.D., *Kaplan's Functional and Surgical Anatomy of the Hand.* Philadelphia, PA: J.B. Lippincott Company, 1984.

[14] D.E. Thompson and D.J. Giurintano, "A kinematic model of the flexor tendons of the hand," *J. Biomechanics*, vol. 22, pp. 327-334, 1989.

[15] D.E. Whitney, "The mathematics of coordinated control of prosthetic arms and manipulators," *ASME J. Dynamic Systems, Meas., Control*, pp. 303-309, 1972.

[16] H.J. Woltring, R. Huiskes and A. DeLange, "Finite centroid and helical axis estimation from noisy landmark measurements in the study of human joint kinematics," *J. Biomechanics*, vol. 18, pp. 379-389, 1985.